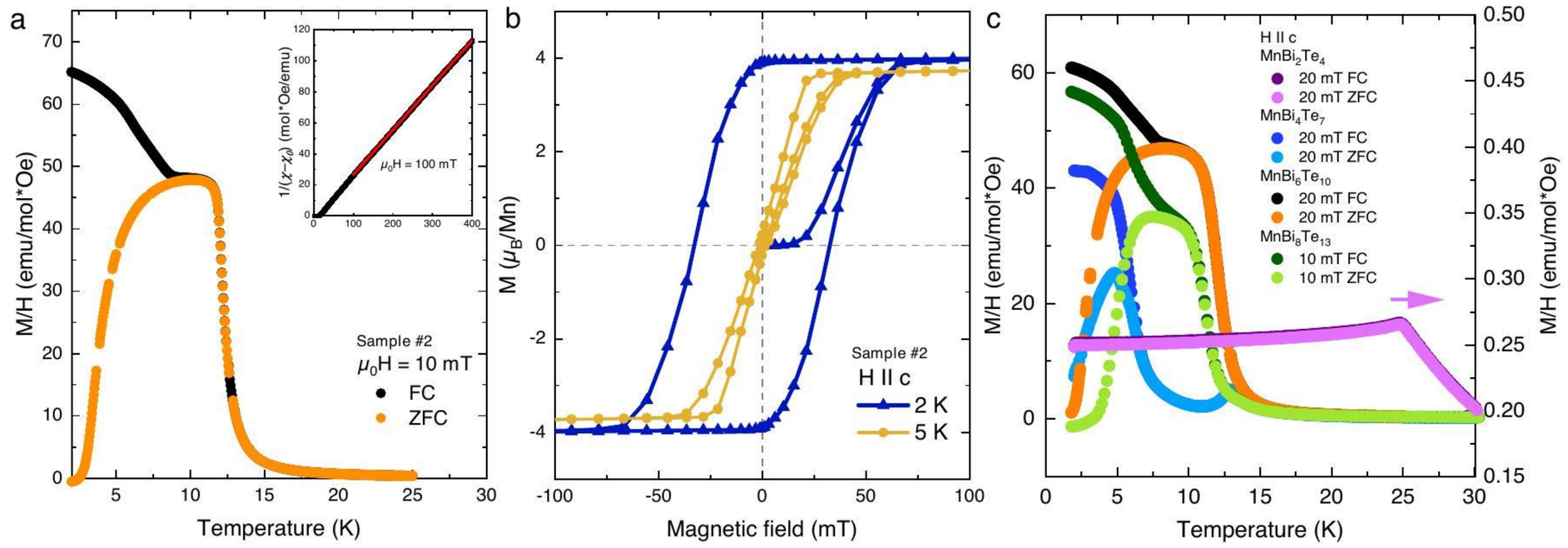

FIG. 2. SQUID magnetometry measurements. (a) Temperature-dependent normalized magnetization M/H of sample #2 with ZFC (orange symbols) and (FC (black symbols) protocols in an out-of-plane applied magnetic field of 10 mT. The inset shows the inverse magnetic susceptibility in a magnetic field of 100 mT together with a modified Curie-Weiss fit $\chi(T) = \chi_0 + C/(T - \Theta_{\mathrm{CW}})$ of the data above 100 K (red solid line); for details see the Methods section. (b) Field-dependent magnetization of sample #2 measured in an out-of-plane applied magnetic field at $T = 2$ K and 5 K. No demagnetization correction was applied, and the magnetization was normalized to the Mn content obtained by EDX. (c) Temperature dependence of the normalized magnetization of analogously synthesized samples of the MBT_n family for $(n = 0, 1, 2, 3)$.

ber of quintuple Bi_2Te_3 layers n increases: $MnBi_2Te_4$ ($n = 0$) has a clear A-type AFM structure, whereas $MnBi_4Te_7$ ($n = 1$) exhibits a more complex behavior, in which robust low-temperature metamagnetic properties are established, which were shown to result from the competition between the uniaxial anisotropy K and the still sizable interlayer AFM interaction J [21]. Finally, in $MnBi_6Te_{10}$ ($n = 2$), as well as in $MnBi_8Te_{13}$ ($n = 3$), the FM properties clearly dominate, with FM order at the significant temperatures of $T_c = 12$ K and 10 K, respectively. Consistent with this observation, the spin-flop transition found for $MnBi_2Te_4$ and $MnBi_4Te_7$ at fields of 3.5 T [32, 35, 36] and 0.1–0.3 T [23, 26, 33, 37], respectively, is absent in $MnBi_6Te_{10}$, and a magnetic moment of more than $4\mu_B$ is observed already above 80 mT in the latter after a ZFC procedure.

C. Bulk DFT (GGA+U) calculations

We have first performed fully relativistic DFT calculations based on the Generalized Gradient Approximation (GGA)+U [38] for $MnBi_6Te_{10}$ neglecting the intermixing. For the interaction parameters, we have used the Slater integrals in Table I for the initial state. The results of total energy calculations for the A-type AFM configuration favor the out-of-plane over the in-plane magnetization by ~ 0.4 meV per Mn. Additional calculations indicate that the A-type AFM configuration has a lower energy than the FM configuration. However, the small magnitude of the difference, ~ 0.04 meV per Mn, naturally suggests that other mechanisms such as Mn/Bi intermixing may well be relevant for the magnetic ground state.

Taking into account the Mn/Bi intermixing for $MnBi_6Te_{10}$, with its lattice parameter $c > 100$ Å, would require a prohibitively long computational time. Instead, here we aim to learn the effects of Mn/Bi intermixing on magnetism via the simpler models of $MnBi_2Te_4$ and $MnBi_4Te_7$. The latter case is more representative of $MnBi_6Te_{10}$, since it contains both SLs and QLs, and is discussed in detail below, while the former is presented in the Supporting Information (Sec. IIIA). Here, we emphasize one conclusion about $MnBi_2Te_4$: even though its defect-free form has the strongest AFM coupling between Mn in the consecutive SLs, based on our calculations, intermixing can induce the FM order between the SLs even in this compound (Fig. S5 in the Supporting Information). Hence, the emergence of strong out-of-plane FM correlations due to the intermixing is likely to be universally present in the MBT_n family, including $MnBi_6Te_{10}$.

As n increases, the possibilities for intermixing patterns naturally become larger as antisite Mn atoms can be located in the 6c positions (occupied by Bi in the defect-free case) of both the SLs and the QLs. $MnBi_4Te_7$ provides the minimal framework to explore whether this enlarged configuration space can yield variations in the experimentally observed ground states. We have performed scalar-relativistic calculations for various intermixing patterns and magnetic orders in a $2 \times 1 \times 2$ supercell of $MnBi_4Te_7$ (Fig. 3). In addition to the defect-free case (S_0), we construct models (S_1 to S_{15}) with different Mn/Bi antisite defects, all of them globally stoichiometric and having a 50% fraction of Bi atoms in the 3a Wyckoff site. Notice that this concentration is close to the outcome of our Rietveld refinements ($\sim 44\%$). The models differ in the positions occupied by the antisite Mn atoms and can be classified into three categories. In the first category, the antisite Mn atoms reside in the 6c position of *only* the QLs (S_1 to S_4). Similarly, in the second cate-